



# Study of the physical mechanism of a solar flare by MHD simulation above the active region: the appearance of extended surface of magnetic lines passing through a chain of current density maxima

A.I. Podgorny<sup>1</sup> and I.M. Podgorny<sup>2</sup>

<sup>1</sup> Lebedev Physical Institute of the Russian Academy of Sciences, Leninsky Prospect 53, Moscow, 119991, Russia

<sup>2</sup> Institute of Astronomy of the Russian Academy of Sciences, Pyatnitskaya Str. 48, Moscow, 119017, Russia

**Abstract.** The primordial release of solar flare energy in the corona at altitudes of 15,000 - 70,000 kilometers is explained by the physical mechanism of S.I. Syrovatsky, based on fast release of the energy accumulation in the magnetic field of the current sheet. The fast release of the magnetic energy of the current sheet leads to the observed manifestations of the flare, which are explained by the electrodynamic model of the solar flare proposed by I. M. Podgorny. The model uses analogies with the electrodynamic model of a substorm, previously developed by its author. Since it is impossible to obtain the configuration of the magnetic field in the corona from observations, it is necessary to carry out MHD simulations. When setting the problem, no assumptions were made about the mechanism of the solar flare. For a numerical solution, the upwind absolutely implicit finite-difference scheme, conservative with respect to the magnetic flux, has been developed. The scheme is realized in the PERESVET computer program. A detailed study of pre-flare state above the active region AR 10365 was performed. The study showed appearance of extended current sheet 50,000 km wide, which is surface of magnetic lines passing through the chain of closely spaced current density maxima. Magnetic lines of the surface have shape of arches located in bright region of the flare radiation. At the center of such a current sheet, 3D maximum of current density does not necessarily have to be achieved. Appearance of a flare in such an arcade is explained by the fact that main part of the surface of magnetic arcs has properties that contribute to development of flare instability.

**Keywords:** solar flare; current sheet; MHD simulation; active region

**DOI:** 10.26119/VAK2024-ZZZZ

# 1 Introduction

Primordial energy release of the solar flare takes place in the solar corona at the altitude 15 000 km - 70 000 km (1/40 - 1/70 of the Solar radius). Proof of this is the appearance of a source of flare thermal X-ray emission on the limb (Lin et al. 2003). Also this follows from numerous observations (see for example (Podgorny et.-al 2015; Podgorny and Podgorny 2018, 2019)) and is confirmed by the results of numerical MHD simulation above the active region (Podgorny and Podgorny 2008; Podgorny et.-al 2023; Jiang et.-al 2016).

The appearance of flare high in the corona is explained by the solar flare mechanism proposed by S.I. Syrovatsky, according to which, the energy accumulated in the magnetic field of the current sheet is released (Syrovatskii 1966). A current sheet is created in the vicinity of the X-type singular line of magnetic field as a result of plasma movement under the influence of magnetic forces  $\mathbf{j} \times \mathbf{B}/c$  (Figure 4 of the Presentation). During the process of quasi-stationary evolution, the current sheet transfers into an unstable state (Figure 5 of the Presentation). The instability leads to the explosive release of the magnetic energy of the sheet with observable manifestations of the flare, which are explained by the electrodynamic model of the solar flare proposed by I. M. Podgorny (Podgorny et.-al 2010). The force of magnetic tension along the sheet accelerates, first of all, electrons that carry electric current. The Hall electric field  $\mathbf{j} \times \mathbf{B}/c$ , resulting from the appeared charge separation, generates an electric current circuit of two field-aligned currents along magnetic lines exiting from the current sheet, which are closed by the Petersen current on the photosphere. Electrons accelerated in field-aligned currents produce beam hard X-ray emission with energies of 50-100 keV in the lower dense layers of the solar atmosphere. The electrodynamic model of solar flare uses analogies with the electrodynamic model of substorm, previously proposed by its author based on measurements on the "Intercosmos-Bulgaria-1300" spacecraft (Podgorny et.-al 1988).

Since it is impossible to obtain the configuration of the magnetic field in the corona from observations, to study the flare situation it is necessary to carry out MHD simulations in the solar corona. When setting the problem, no assumptions were made about the mechanism of the solar flare. All conditions were taken from observations. The problem was set to determine the mechanism of a solar flare from the results of numerical MHD simulation. To study the physical mechanism of a solar flare, calculations must begin several days before the flare, when magnetic energy for the flare has not yet accumulated in the corona.

## 2 Setting of the problem

MHD simulation is carried out above the active region AR 10365 during the time interval from 24.05.2003 20:48 to 27.05.2003 20:48. The computational domain in the corona is a rectangular parallelepiped ( $0 \leq x \leq 1$ ,  $0 \leq y \leq 0.3$ ,  $0 \leq z \leq 1$ ) (the length unit was chosen  $L_0 = 4 \times 10^{10}$  cm). The lower boundary of the computational domain  $y=0$  (XZ) is located on the surface of the Sun (photosphere) and contains the active region; the Y axis is directed from the Sun perpendicular to the photosphere. The X axis is directed from east to west, and the Z axis is from north to south. A typical magnetic field strength in the active region,  $B_0 = 300$  G, was used as the unit of the magnetic field. In this domain, the complete magnetohydrodynamics system for compressible plasma with all dissipative terms was solved :

$$\frac{\partial \mathbf{B}}{\partial t} = \text{rot}(\mathbf{V} \times \mathbf{B}) - \frac{1}{\text{Re}_m} \text{rot}\left(\frac{\sigma_0}{\sigma} \text{rot} \mathbf{B}\right) - \text{rot}(\nu_{m\_Art} \text{rot} \mathbf{B}) \quad (1)$$

$$\frac{\partial \rho}{\partial t} = -\text{div}(\mathbf{V}\rho) \quad (2)$$

$$\begin{aligned} \frac{\partial \mathbf{V}}{\partial t} = & -(\mathbf{V}, \nabla)\mathbf{V} - \frac{\beta}{2\rho} \nabla(\rho T) - \frac{1}{\rho}(\mathbf{B} \times \text{rot} \mathbf{B}) + \frac{1}{\text{Re}_\rho} \Delta \mathbf{V} + \\ & + G_g \mathbf{G} + \nu_{Art} \Delta \mathbf{V} \end{aligned} \quad (3)$$

$$\begin{aligned} \frac{\partial T}{\partial t} = & -(\mathbf{V}, \nabla)T - (\gamma - 1)T \text{div} \mathbf{V} + (\gamma - 1) \frac{2\sigma_0}{\text{Re}_m \sigma \beta \rho} (\text{rot} \mathbf{B})^2 - \\ & - (\gamma - 1)G_q L'(T)\rho + \frac{\gamma - 1}{\rho} \text{div} [\mathbf{e}_{\parallel} \kappa_{dl}(\mathbf{e}_{\parallel}, \nabla T) + \\ & + \mathbf{e}_{\perp 1} \kappa_{\perp dl}(\mathbf{e}_{\perp 1}, \nabla T) + \mathbf{e}_{\perp 2} \kappa_{\perp dl}(\mathbf{e}_{\perp 2}, \nabla T)] \end{aligned} \quad (4)$$

( details in (Podgorny and Podgorny 2008, 2004; Podgorny et.-al 2018) )

Important parameters of the MHD equations are the magnetic Reynolds number  $\text{Re}_m$  and the ordinary Reynolds number  $\text{Re}$ , which determine the predominance of the transfer of the magnetic field and matter over the diffusion spreading due to magnetic viscosity and ordinary viscosity were choosen according to principle of limited simulation (Podgorny 1978) ( $\text{Re}_m = 3 \times 10^4$ ,  $\text{Re} = 10^4$ ).

In order to determine the evolution of the magnetic field in corona by solving the equations of magnetic hydrodynamic (1-4), it is necessary to know the magnetic field in the corona at the initial moment of time and the magnetic field on the photosphere during the time interval of calculation.

The initial magnetic field is taken to be a potential magnetic field that should approximate the corona field well enough at the initial time several days before the

flares occur, when there are no strong disturbances. To set the conditions at the photospheric boundary, it is necessary to know two magnetic field components parallel to the boundary. This is because the magnetic field component normal to the boundary is found from the condition  $\text{div } \mathbf{B} = 0$ , and in the case of using a finite-difference scheme conservative with respect to the magnetic flux, the normal field component is calculated automatically when solving the MHD equations. During the calculated time period, regular distributions of the magnetic field vector have not yet been observed, so the field components necessary for setting the boundary conditions were found from the calculated potential field. This approximation can be used because the magnetic field on the photosphere is determined mainly by currents beneath the photosphere, not in the corona. To determine the potential field in the corona, it is necessary to solve the Laplace equation for the magnetic field potential with the oblique derivative along the line of sight as a boundary condition. The oblique derivative along the line of sight of the magnetic field potential, specified at the boundary, is expressed through the component of the magnetic field along the line of sight. The line-of-sight photospheric magnetic field distribution  $B_{\text{lsight}}$  was taken from the SOHO MDI magnetic field maps (<http://soi.stanford.edu/magnetic/index5.html>). The setting of the problem, which was solved numerically, is as follows:

$$\Delta\varphi = 0; \quad \left. \frac{\partial\varphi}{\partial l_{\text{lsight}}} \right|_{\text{PhBoun}} = -B_{\text{lsight}}; \quad \mathbf{B} = -\nabla\varphi \quad (5)$$

### 3 Developed methods for solving the problem

For the numerical solution of MHD equations, the absolutely implicit upwind finite-difference scheme, conservative relative the magnetic flux, has been developed [(Podgorny and Podgorny 2008, 2004)]. The scheme is solved by the method of iterations. Special methods were developed with the aim of constructing a scheme that remains stable for the maximum possible time step. The scheme was realized in the computer program PERESVET.

The Laplace equation for the magnetic field potential with the oblique derivative (5) to find potential magnetic field is solved by two methods using a finite-difference scheme. In the first of them simple iterations are used, in which the values of the potential in the central point of a stencil is found via the neighboring points at the previous iteration. The second method consists in relaxation of the evolutionary diffusion equation

$$\frac{\partial\varphi}{\partial t} = D\Delta\varphi \quad (6)$$

During solving by the first method the iterations are converged slowly, because the operator of passing from the previous iteration to the current one is weakly contraction operator, e. g. its norm is not much less than unit. Such a method of solving is used in the first turn for checking. The solution obtained by this method is coincided with the solution obtained by the second method. The implicit scheme is used for diffusion equation (6) solving. This scheme is solved by an iteration method at the each time step. To accelerate the calculation a special algorithm is developed, according to which the small number of iteration is performed at first time steps, and further the number of iterations are gradually increased. Decrease of calculation time is achieved due to the diminishing the solution precision of the diffusion equation (6). But the solution precision of the Laplace equation (5), to which the solution of diffusion equation is tended for  $t \rightarrow \infty$ , does not become worse.

Parallelization of calculations was carried out by computational threads on modern graphics cards (GPU) V-100 and Titan-100 using CUDA technology.

For small magnetic and usual viscosities, numerical instabilities arose near the boundary of the computational domain, which were stabilized using the developed methods [(Podgorny et.-al 2023, 2022)].

The magnetic field configuration obtained by MHD simulation is so complex that it is often impossible to determine the positions of special lines and the current sheets appearing near them. For this purpose, a graphical search system [(Podgorny and Podgorny 2013)] was developed, based on determining the positions of the current density maxima, which are achieved in the centers of the current sheets. The current density maxima are located on singular lines of the magnetic field.

## 4 Magnetic field configurations near the founded singular lines and current sheets

Examples of magnetic field configurations in the plane and in space in the vicinity of the found current density maxima are shown in Figure 1. The X-type magnetic field configuration is formed by the so-called "plane" magnetic lines, i.e. lines tangent to the projections of the magnetic field vectors onto the plane of the current sheet configuration. It is this plane configuration that determines the possibility of the appearance of  $\mathbf{j} \times \mathbf{B}/c$  forces that create plasma flows that deform the field into the current sheet configuration. The important role of the plane configuration appears due to the direction of the main part of the current along a special line perpendicular to the configuration plane. As a result, the main components of the magnetic field that determine the  $\mathbf{j} \times \mathbf{B}/c$  magnetic forces lie in the plane of the magnetic field configuration, and the main  $\mathbf{j} \times \mathbf{B}/c$  forces are located in the plane

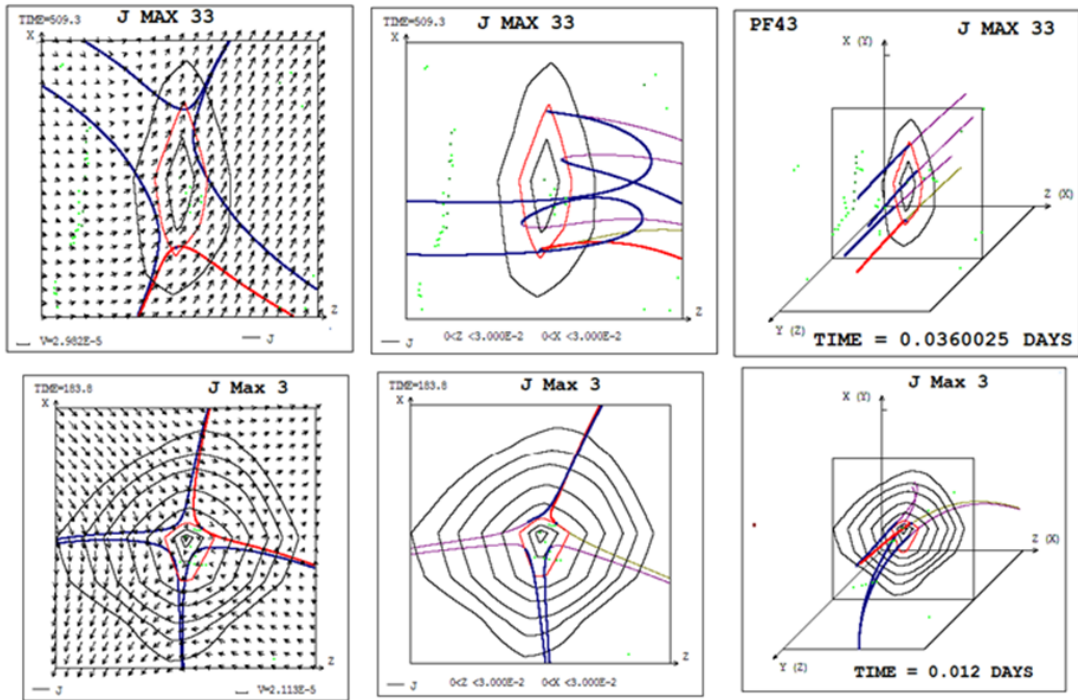


**Fig. 1.** Examples of magnetic field configurations in the vicinity of points on singular lines found by the graphical search system based on the results of MHD simulation.

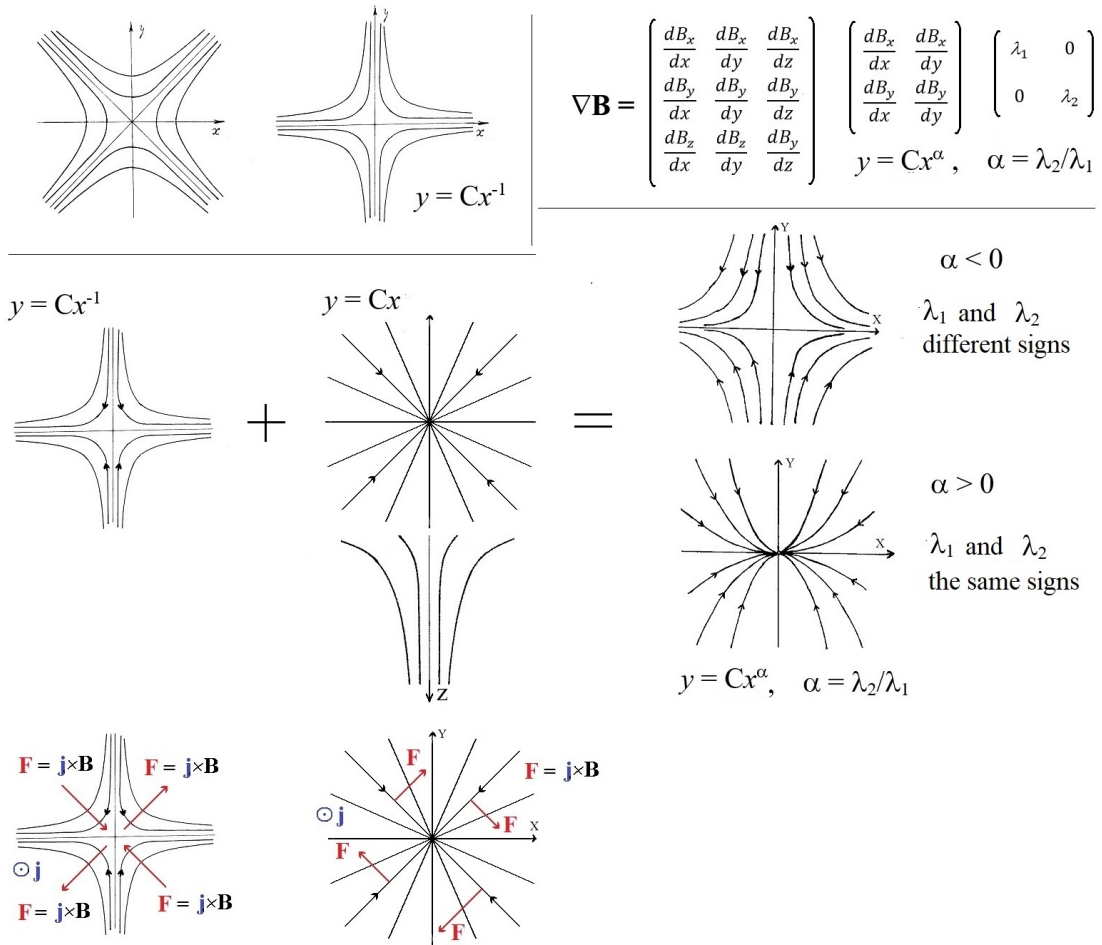
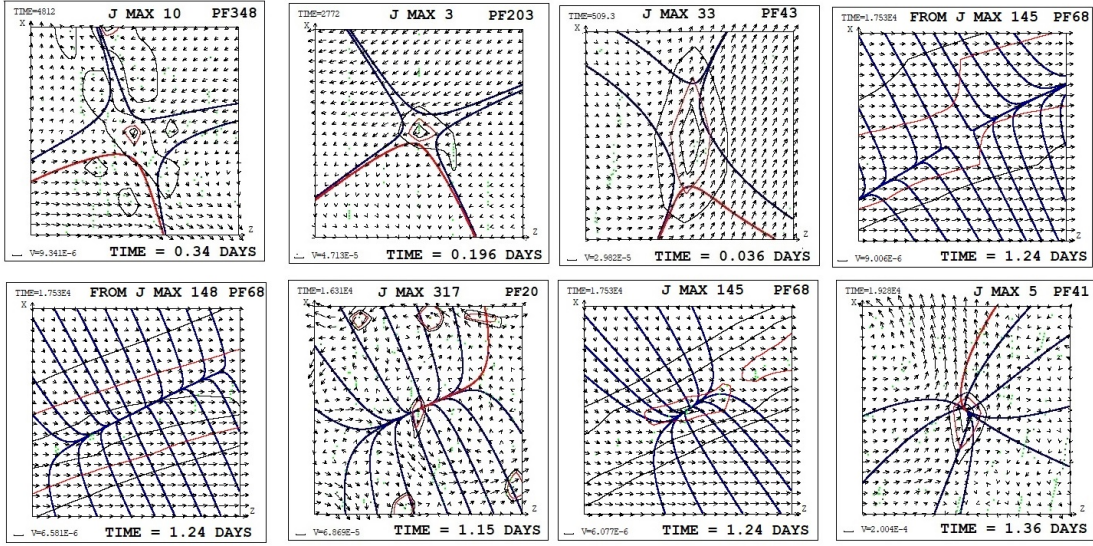


Fig. 2. Overlay of a diverging magnetic field on an X-type field in the vicinity of a singular line.



**Fig. 3.** Examples of plane configurations in the vicinity of singular lines, with the superposition of an X-type field and a diverging magnetic field obtained by the graphical search system based on the results of MHD simulation.

of the configuration perpendicular to the projections of the magnetic field vectors onto the configuration plane, i.e. perpendicular to the "plane" magnetic lines shown in the Figure (first column of Fig. 1). The projections of three-dimensional magnetic lines onto the configuration plane can also form an X-type configuration if the field varies weakly along the singular line, but can represent a configuration that does not resemble a singular line at all. In three-dimensional space, magnetic lines can diverge significantly along the singular line (along the coordinate perpendicular to the plane of the current sheet configuration), so that the magnitude of the field in the plane is relatively large relative to the magnitude of the longitudinal magnetic field. Also, magnetic lines in three-dimensional space can be close to parallel, which means a relatively large longitudinal component of the magnetic field, which will stabilize the instability of the current sheet, thereby preventing the flare release of magnetic energy.

In the vicinity of the singular magnetic field line, a divergent magnetic field can be superimposed on the X-type configuration (Fig. 2), which is a magnetic mirror field (magnetic trap field) created in plasma installations designed to study the possibility of implementing thermonuclear fusion. If the X-type magnetic field predominates, then the superposition will result in a deformed X-type configuration, otherwise a deformed divergent field will result. The divergent field hinders the formation of a

current sheet in the X-type configuration, since it creates a rotational motion around the special line. This rotational motion is not a strong hindrance to the creation of a current sheet: even in the case of a predominance of the divergent magnetic field, since a sufficiently powerful current sheet can be formed due to the presence of the X-type configuration. However, the conditions for a flare are more promotable when the X-type field dominates, since the divergent magnetic field hinders both the formation of a current sheet and the development of instability that leads to a flare-induced energy release. The divergent field prevents the rapid plasma outflow from the sheet under the action of magnetic tension, while this rapid plasma outflow violates the balance of magnetic and gas-dynamic pressures in the sheet, leading to an explosive energy release. Figure 3 shows examples of superpositions of the X-type configuration and the divergent magnetic field obtained from MHD simulations. The divergent field can significantly dominate, in other cases the X-type field can significantly dominate. Also, when superimposed, the divergent field or the X-type field can dominate weakly. A situation can arise in which the influence of the fields of both types is almost equal, while the X-type configuration or the divergent field dominates very weakly.

## 5 Results of MHD simulation: Extended surface of magnetic lines passing through the chain of current density maxima

The detailed study of pre-flare state above the active region AR 10365 at 02:32:05 on May 26, 2003, three hours before the M 1.9 flare was carried out by comparing the results of numerical MHD simulation in the corona with observations of radio emission at a frequency of 17 GHz obtained at the Nobeyama Radioheliograph (NoRH).

The detailed study of the pre-flare situation above the active region AR 10365 at 02:32:05 on May 26, 2003, three hours before the M 1.9 flare by comparing the results of MHD simulations with observations of microwave radio emission at 17 GHz obtained from the Nobeyama Radioheliograph (NoRH) is performed. In this moment the energy for solar flare is accumulated in the magnetic field and plasma of solar corona is heated by currents which creates this magnetic field. Magnetic field configuration is represented by lines passing through maxima of current density with the numbers 145, 147, 194, 179, 4, 73, 105, 41, 12, 205, 123, 82, 84, 182 (Fig. 4.). All current density maxima found by the graphical search system for flare positions numbered in descending order of the current density value at the maximum.

3D magnetic lines in the computational domain in the corona, and projections of magnetic lines onto the central plane of the computational domain (plane passing

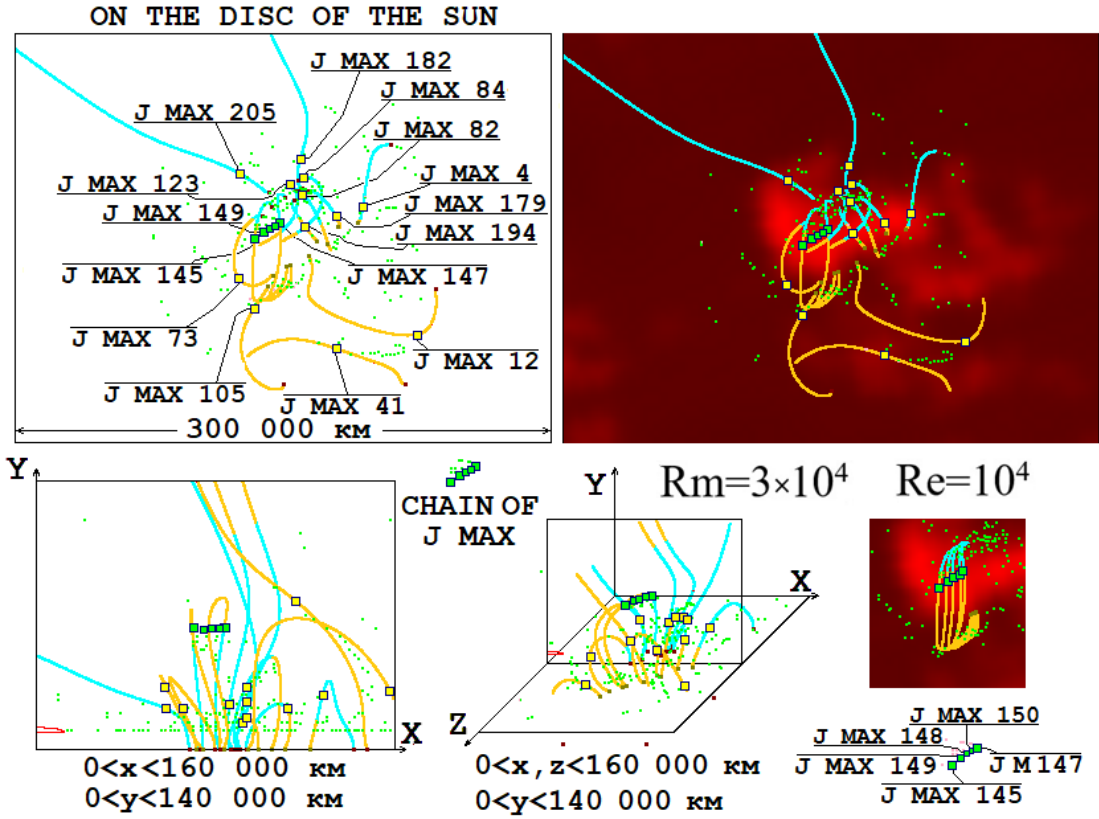


**Fig. 4.** Positions of current density maxima in the computation domain of the corona in space, and their projections onto the central plane of the computation domain and onto the picture plane (perpendicular to the line of sight). The distribution of microwave radio emission at a frequency of 17 GHz, obtained on the solar disk using the Nobeyama radioheliograph, is superimposed on the picture plane. The magnetic field configuration is represented by magnetic lines passing through the selected current density maxima, and their projections onto the planes. The chain of maxima consists of points marked in green.

through the center of the computational domain, located parallel to the solar equator and perpendicular to the solar surface) are shown. Also, the intensity distribution of microwave radiation at a frequency of 17 GHz observed on the solar disk using the Nobeyama radioheliograph (NoRH) is superimposed on the projections of magnetic lines onto the picture plane (perpendicular to the line of sight).

Magnetic field configurations at selected current density maxima points indicate promotable conditions for flare occurrence at some maxima located in the region of bright flare emission. There is no significant dominance of the diverging magnetic field in the vicinity of these maxima. At the same time, maxima with such properties also occur outside the bright region of flare emission, and there are not many such maxima in the bright region compared to their total number.

The problem of coincidence of bright flare emission regions with flare positions found from MHD simulation results can be solved by the occurrence of the surface of high current density, the current passing through a chain of current density maxima. The maxima of this chain with numbers 145, 149, 148, 150 and 147 in Figure 4 are shown by green dots. Magnetic lines on the solar disk passing through the maxima of this chain are shown separately on an enlarged scale.

Figure 5 shows the plane and three-dimensional configurations near the chain maxima in a square and in a cube of 12,000 km. The two-dimensional region is a square of 12,000 km in size with the center at the point of the selected current density maximum, with the plane of the square located perpendicular to the magnetic field vector at the point of the selected maximum (perpendicular to the magnetic line passing through the point of the selected maximum). The three-dimensional region is a cube 12,000 km in size centered at the point of the selected maximum of current density, so that the two-dimensional region is the central plane of this cube, i.e. a plane passing through the center of the cube parallel to two faces of the cube and, accordingly, perpendicular to the other four faces of the cube.

These configurations do not have properties that could significantly promote the flare release of energy. In plane configurations, the divergent magnetic field dominates over the X-type field, although not very strongly, and in three-dimensional configurations, the field lines do not diverge much along the singular line, which means a comparatively large longitudinal component of the magnetic field stabilizing the explosive instability.

The chain maxima are located close to each other and the field configurations in their vicinity are very similar, so that an assumption arises that all the chain maxima belong to the same current sheet of considerable width ( 50,000 km), i.e. an extended surface with an increased current density. This assumption is confirmed by the study of plane and three-dimensional configurations in a square and in a cube with a larger

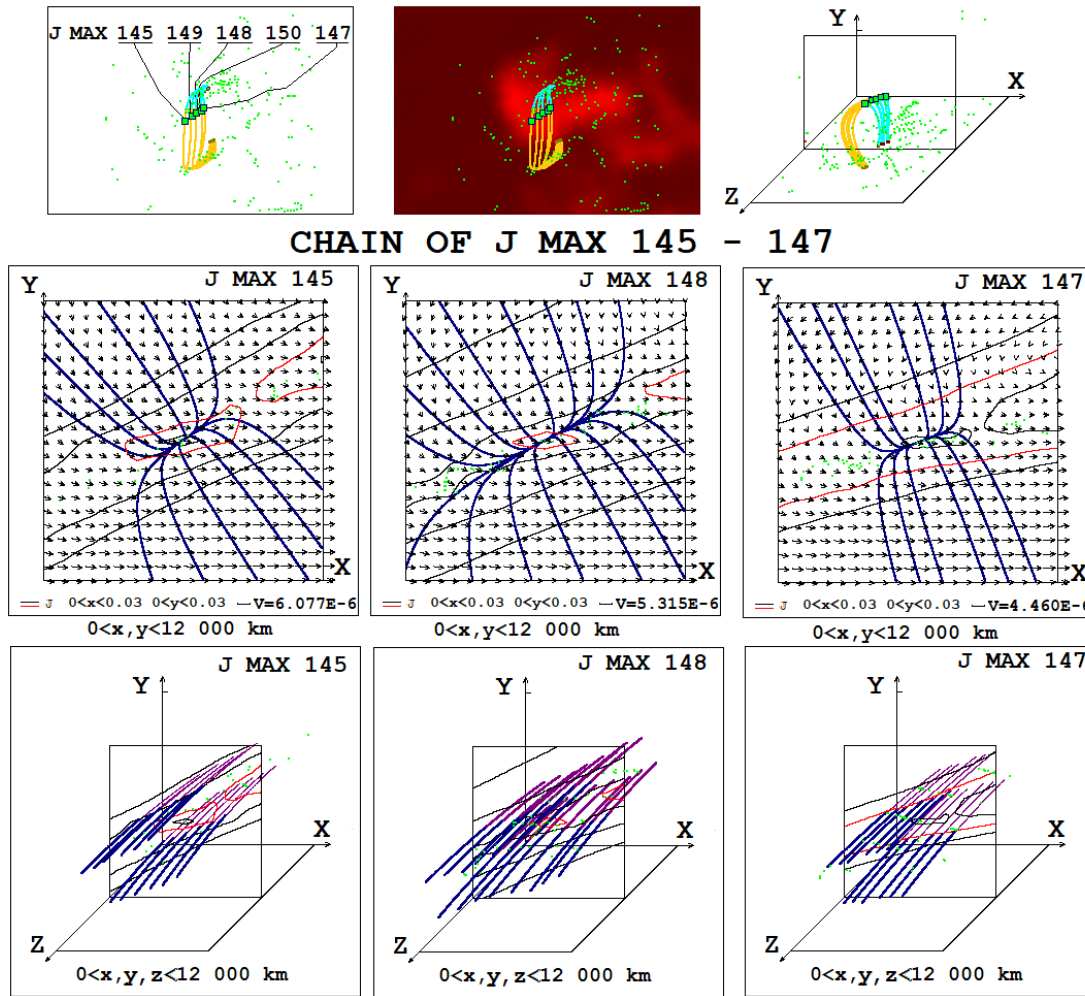


**Fig. 5.** Plane and spatial configurations in regions of 12,000 km in size with centers at the points of the chain of maxima.

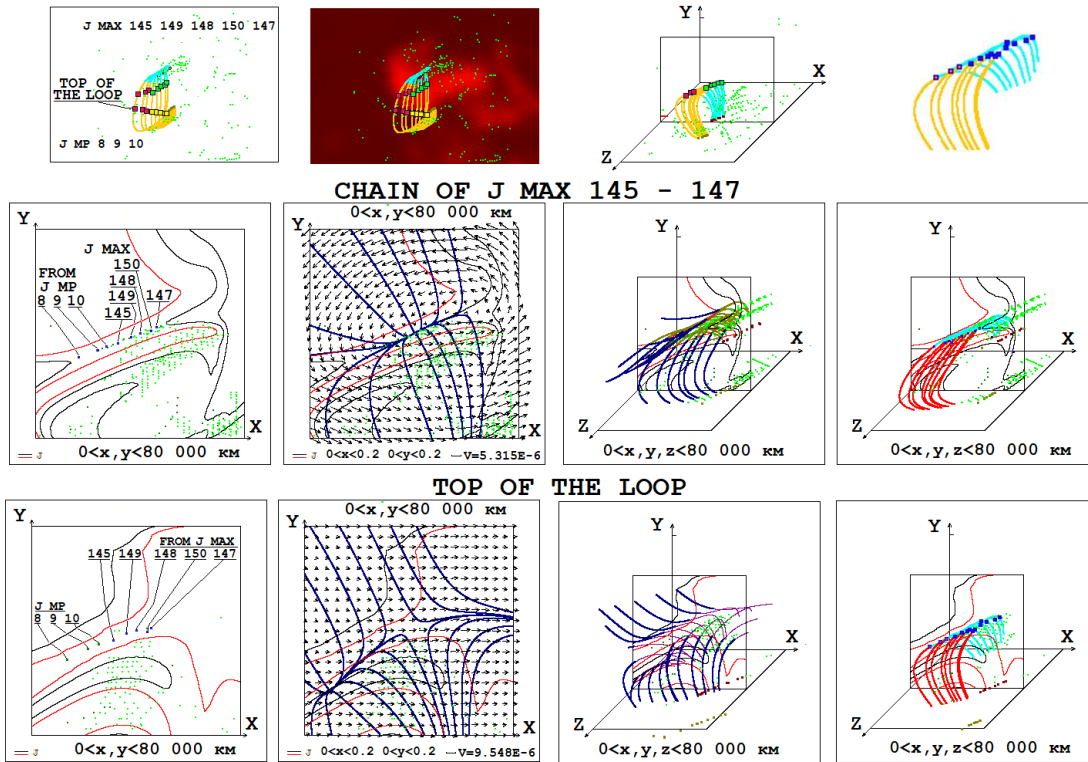


**Fig. 6.** Plane and spatial configurations in large regions of 80,000 km. In the central part of one of these regions there is a chain of maxima. In the central part of another region there are points at the top of an arch located on magnetic lines coming out from the points of the chain of maxima.

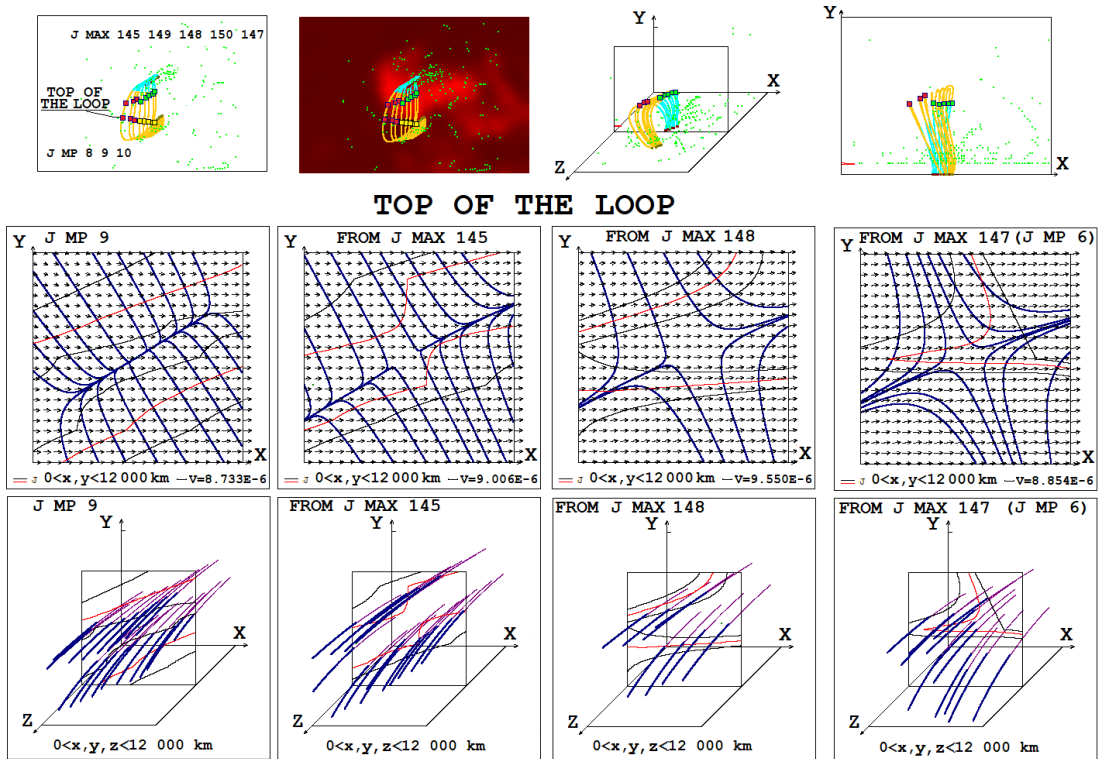


**Fig. 7.** Plane and spatial configurations in regions of 12,000 km in size with centers at the points at the top of the arch located on magnetic lines coming out of the points of the chain of maxima.

size of 80,000 km with the center at the 148th maximum located in the middle of the chain (Figure 6, second row). The square is the central plane of the cube. Magnetic lines in a cube passing through the chain maxima form an arcade (Figure 6, the last figure of the second row).

The current density maxima are not located at the loop top. It is necessary to construct a magnetic configuration at the top of the loop, where, from general considerations about the field configuration with sources under the solar surface, there should be practically no diverging field superimposed on the X-type field, and where, judging by the available observations, solar flares most likely occur. Such a construction is also necessary to check the coincidence of the surface of magnetic lines passing through the chain of current density maxima with the surface of increased current density.

In the upper rows of Figures 6 and 7, the chain maxima points are marked in green, and the points lying on the tops of the loop are marked in yellow. These points at the top of the arcade are obtained as follows. On the magnetic line passing through the central maximum of the chain with the number 148, a point is sought at which the magnetic field vector is parallel to the solar surface (the component of the vector perpendicular to the solar surface is zero). This is the point at the top of the loop on the central line. A large region of 80,000 km is constructed with the center at this point. The plane of the square with the center at this point is perpendicular to the magnetic vector and is the central plane of a large cube.

The points on the solar disk and in the calculated region of the corona at the loop tops, marked in yellow, are the intersection points of the magnetic lines passing through the chain maxima with the constructed central plane. These points lie in the region of increased current density, as can be seen from their location in the central plane, on which the current density level lines are plotted, which confirms the coincidence of the surface of the lines passing through the chain maxima with the surface of increased current density (Fig. 6, first figures of the second and third rows). In the region of increased current density in the central plane, the intersection points of the magnetic lines passing through the chain maxima with this central plane are plotted, designated as FROM J MAX 145, 149, 148, 150, 147 and flat maxima J MP 8, 9, 10, which do not coincide with these intersection points FROM J MAX (some flat maxima coincide with the points FROM J MAX). In the upper rows of Figures 6 and 7 in the picture plane on the solar disk and in the calculation area the points of these plane maxima are marked in red, magnetic lines are drawn through them. The points of intersection of these lines with the central plane of the chain of maxima are also marked in red in the lower part of the figure. These eight lines, five of which pass through the maxima of the chain, and three through the flat maxima

of the current density, represent an arcade, which is depicted in a large cube (80,000 km) with the center at the point on the top of the arcade (Fig. 6, last figure of the third row).

Magnetic field configurations (Fig. 7) in the vicinity of the loop top points in the central plane of 12,000 km in size have properties that promote the development of flare instability. In most of these small regions, the X-type field dominates, while in other regions, the diverging field dominates very weakly. In the three-dimensional configuration, the field lines diverge significantly in the direction along the singular line, which means that the longitudinal component of the magnetic field is relatively weak, so that it will not be able to stabilize flare instability.

Comparison of two-dimensional and three-dimensional configurations in small regions of 12,000 km in size for the points of the chain of maxima and the points at the top of the arcade (Fig. 5 and Fig. 7) shows a much more promotable situation for the occurrence of flare instability at the loop tops, rather than at the points of the chain maxima. The same result is obtained by comparing the magnetic field configurations in large regions (80,000 km in size) at the location of the chain of maxima and at the top of the arch (Fig. 6)

## 6 Discussion and conclusion

Thus, the occurrence of a surface of increased current density located on magnetic lines passing through a chain of current density maxima can solve the problem of coincidence regions of bright flare radiation with the positions of flares found from the results of MHD simulation using a graphical search system based on the search for current density maxima. During flares, the energy of the magnetic field of the current located on the surface of increased current density can be released. This surface of increased current density is an arcade of magnetic lines passing through a chain of current density maxima. In fact, this surface is an extended current sheet.

The instability leading to the main energy release of the flare can begin at the top (or near the top) of the arcade, where current density maxima may not appear. However, the current density in this place is large enough, differing little from the current density in the maxima located far from the top of the arcade. Also, flat current density maxima can be located at the tops of the arcades, in a plane perpendicular to the magnetic vector. The reason for the appearance of flare instability at the top of the arcade is the properties of the magnetic field configuration in this place, which promote to the occurrence of instability of the current sheet (the dominance of the X-type field and the significant divergence of magnetic lines in three-dimensional space along the direction of the special line, which means a small value of the longitudinal

component of the current sheet). Further, the instability can spread to the entire region of the current sheet, which is confirmed by the location of the entire arcade with an increased current density in the region of bright flare radiation.

The appearance of current density maxima with magnetic field configuration properties, that promote flare instability, outside the bright flare region can be explained by the location of these magnetic field features out of the powerful arcade with increased current density, due to which much energy will not accumulate in the resulting current sheet.

The proposed solution to the problem of the coincidence of the flare position found from the results of MHD simulation with the bright region of flare (or pre-flare) emission needs further verification. This verification should be carried out by carefully searching for all features of the magnetic field found by MHD simulation and comparing the position of these features with the position of the bright region for this moment and other moments of the selected flare and other flares.

**Acknowledgements.** The authors are grateful to the SOHO/MDI (Michelson Doppler Imager on the spacecraft Solar and Heliospheric Observatory) team and the Nobeyama radioheliograph team (The Nobeyama Radio Observatory, the division of the National Astronomical Observatory of Japan, located near Minamimaki, Nagano at an elevation of 1350 m.) for the scientific data provided as well as to the many professional cloud service specialists who made it relatively easy for us to configure rented remote computers for GPU computing.

## References

1. Lin, R.P., Krucker, S., Hurford, G.J., et al. 2003, *Astrophys. J.*, v. 595, Issue 2, pp. L69-L76.
2. Podgorny, A.I., Podgorny, I.M., Meshalkina, N.S. 2015, *Astron. Rep.*, v. 59, Issue 8, pp. 795-805.
3. Podgorny, I.M., Podgorny, A.I. 2018, *Astron. Rep.*, v. 62, Issue 10, pp. 696-704.
4. Podgorny I.M. and Podgorny A. I. 2019, *Sun Geosph.*, v. 14, No 1. pp. 13-19.
5. Podgorny, A.I., Podgorny, I.M. 2008, *Astron. Rep.*, v. 62, Issue 8, pp. 666-675
6. Podgorny, A.I., Podgorny, I.M., Borisenko, A.V. 2023, *Physics*, v. 5, No. 3, pp. 895-910.
7. Syrovatskii, S.I. 1966, *Sov. Phys. JETP*, v. 23, No. 4, pp. 754-762.
8. Podgorny, I.M., Balabin, Y.V., Vashenyuk, E.V., Podgorny, A.I. 2010, *Astron. Rep.*, v. 54, Issue 7, pp. 645-656.
9. Podgorny, I.M., Dubinin, E.M., Israilevich, P.L., Nicolaeva, N.S. 1988, *Geophys. Res. Lett.*, v. 15, Issue 13, pp. 1538-1540.
10. Podgorny, I.M. 1978, *Fundam. Cosm. Phys.*, v. 4, pp. 1-72.
11. Podgorny, A.I., Podgorny, I.M. 2004, *Math. Math. Phys.*, v. 44, Issue 10, pp. 1784-1806.
12. Podgorny A.I. and Podgorny I. M. 2013, *Sun Geosph.*, v. 8, No 2. pp. 71-76.

13. Jiang C., Wu S.T., Yurchyshyn V., Wang H., Feng X., Hu Q. 2016. *Astrophys. J.*, v. 828. No. 1. article id. 62, 12 pp.
14. Podgorny, A.I., Podgorny, I.M., Meshalkina, N.S. *Journ. Atm. Solar-Ter. Phys.*, 180, pp. 16-25 (2018)
15. Podgorny, A.I., Podgorny, I.M., Borisenko, A.V. 2022. *Open Astron.*, v. 31, pp. 27-37.